

Asymptotic behavior of the order parameter in a stochastic sandpile

Ronaldo Vidigal* and Ronald Dickman†

*Departamento de Física, ICEx, Universidade Federal de Minas Gerais,
30123-970 Belo Horizonte - Minas Gerais, Brazil*

(January 18, 2019)

Abstract

We derive the first four terms in a series for the order parameter (the stationary activity density ρ) in the supercritical regime of a one-dimensional stochastic sandpile; in the two-dimensional case the first three terms are reported. We reorganize the perturbation theory for the model, recently derived using a path-integral formalism [R. Dickman e R. Vidigal, *J. Phys. A* **35**, 7269 (2002)], to obtain an expansion for stationary properties. Since the process has a strictly conserved particle density p , the Fourier mode $N^{-1}\psi_{k=0} \rightarrow p$, when $N \rightarrow \infty$, and so is not a random variable. Isolating this mode, we obtain a new effective action leading to an expansion for ρ in the parameter $\kappa \equiv 1/(1+4p)$. This requires enumeration and numerical evaluation of more than 200 000 diagrams, for which task we develop a computational algorithm. Predictions derived from this series are in good accord with simulation results. We also discuss the nature of correlation functions and one-site reduced densities in the small- κ (large- p) limit.

*E-mail: rvidigal@dedalus.lcc.ufmg.br

†E-mail: dickman@fisica.ufmg.br

I. INTRODUCTION

Sandpiles are the principal examples of self-organized criticality (SOC) [1–5]. Sandpiles with a strictly conserved particle density (so-called *fixed-energy sandpiles* or FES [6]), exhibit an absorbing-state phase transition [7–9], rather than SOC, and have recently attracted much interest. Until now, most quantitative results for FES have been based on simulations [10–15], an important exception being the solution by Priezzhev *et al.* [16] of a directed, fixed-energy version of the Maslov-Zhang model [17], via the Bethe ansatz. Recently, a time-dependent perturbation theory based on the path-integral formalism was derived for a stochastic sandpile [18]. In [19] the series expansion for the one-dimensional case was extended using operator methods.

In the present work, the perturbation theory developed in [18] will be reformulated, leading to an expansion for stationary ($t \rightarrow \infty$) properties instead of the short-time expansion obtained previously. The expansion parameter is $\kappa \equiv 1/(1 + 4p)$, where p denotes the particle density, a conserved quantity.

Our analysis depends on two basic tools. One is an operator formalism for Markov processes, of the kind developed by Doi [20], and which has been applied to various models exhibiting nonequilibrium phase transitions [21–25]. The second is an exact mapping, devised by Peliti, of a Markov process to a path-integral representation [26,27]. This approach is frequently used to generate the effective action corresponding to a process, for subsequent analysis via renormalization group (RG) techniques. In the present instance our immediate objective is not a RG analysis but an expansion for the order parameter. In the path-integral formalism the probability generating function is written in terms of functional integrals over the fields $\psi(x, t)$ (whose expectation is the particle density at site x), and an auxiliary field $\bar{\psi}(x, t)$. Our reformulation of the effective action is based on the observation that, due to particle conservation, the Fourier mode $N^{-1}\psi_{k=0}$ is not a random variable, but rather has the fixed value p when N , the number of lattice sites, goes to infinity.

We consider Manna’s stochastic sandpile in its fixed-energy (particle-conserving) version [12,18,28,29]. The configuration is specified by the occupation number n at each site; sites with $n \geq 2$ are said to be *active*, and have a positive rate of *toppling*. When a site topples, it loses exactly two particles (“grains of sand”), which move randomly and independently to nearest-neighbor (NN) sites. (Any configuration devoid of active sites is *absorbing*, i.e., no further evolution of the system is possible once such a configuration is reached.) In this work, as in [18,19], we adopt a toppling rate of $n(n-1)$ at a site having n particles, which leads us to define the order parameter as $\rho = \langle n(n-1) \rangle$. While this choice of rate represents a slight departure from the usual definition (in which all active sites have the same toppling rate), it leads to a much simpler evolution operator, and should yield the same scaling properties [18]. Preliminary simulation results [30] indicate that in one dimension the model exhibits a continuous phase transition at $p_c = 0.9493$.

The balance of this article is organized as follows. In Sec. 2, we discuss the reorganization of the action, and in Sec. 3 develop a perturbation expansion for the activity density in the supercritical regime. Sec. 4 presents the diagrammatic expansion rules and the resulting expansion. Predictions for the activity density are reported and compared against simulation in Sec. 5, while in Sec. 6 we examine correlation functions and higher moments of the density. In Sec. 7 we present a brief discussion of our results.

II. EFFECTIVE ACTION

As shown in [18], the master equation for the stochastic sandpile can be written in the form

$$\frac{d|\Psi\rangle}{dt} = L|\Psi\rangle, \quad (1)$$

where

$$|\Psi\rangle = \sum_{\{n_i\}} p(\{n_i\}, t) |\{n_i\}\rangle, \quad (2)$$

where $p(\{n_i\}, t)$ is the probability of the configuration having occupation numbers $\{n_i\}$ and $|\{n_i\}\rangle$ is the direct product of states $|n_j\rangle$, representing exactly n_j particle at site j . In one dimension, the evolution operator takes the form

$$L = \sum_i \left[\frac{1}{4}(\pi_{i-1} + \pi_{i+1})^2 - \pi_i^2 \right] a_i^2 \equiv \sum_i L_i. \quad (3)$$

Here a_i e π_i are, respectively, destruction and creation operators associated with site i , defined via

$$a_i |n_i\rangle = n_i |n_i - 1\rangle \quad (4)$$

and

$$\pi_i |n_i\rangle = |n_i + 1\rangle. \quad (5)$$

As shown in [18], the evolution operator in Fourier representation is given by

$$L = -N^{-3} \sum_{k_1, k_2, k_3} \omega_{k_1, k_2} \pi_{k_1} \pi_{k_2} a_{k_3} a_{-k_1 - k_2 - k_3}, \quad (6)$$

with $\omega_{k_1, k_2} = 1 - \cos k_1 \cos k_2$; the sums are over the first Brillouin zone.

As explained in [18], the expectation of any observable $A(\{n_i\})$ can be written in terms of a functional integral

$$\langle A \rangle = \int \mathcal{D}\tilde{\psi} \mathcal{D}\psi \mathcal{A} \mathcal{G}[\psi, \tilde{\psi}], \quad (7)$$

where $\mathcal{A}(\psi, \tilde{\psi})$ is a function of the fields ψ and $\tilde{\psi}$ corresponding to observable A , and

$$\mathcal{G}[\psi, \tilde{\psi}] \equiv \exp \left[-N^{-1} \int_0^t dt' \sum_k \tilde{\psi}_k \dot{\psi}_{-k} + \int_0^t dt' \mathcal{L}_I \right] \equiv \exp \left[-N^{-1} \int_0^t dt' \mathcal{L}_0 + \int_0^t dt' \mathcal{L}_I \right], \quad (8)$$

with the interaction given by

$$\begin{aligned} \mathcal{L}_I = & -N^{-3} \sum_{k_1, k_2, k_3} \omega_{k_1, k_2} \tilde{\psi}_{k_1} \tilde{\psi}_{k_2} \psi_{k_3} \psi_{-k_1 - k_2 - k_3} \\ & - 2N^{-2} \sum_{k_1, k_2} \omega_{k_1, 0} \tilde{\psi}_{k_1} \psi_{k_2} \psi_{-k_1 - k_2}. \end{aligned} \quad (9)$$

The field ψ is closely related to the occupation number [27]. In particular, the activity density is given by

$$\rho(t) \equiv N^{-1} \sum_j \langle n_j (n_j - 1) \rangle = N^{-2} \sum_k \langle \psi_k \psi_{-k} \rangle, \quad (10)$$

while for the particle density we have

$$\phi \equiv N^{-1} \sum_j \langle n_j \rangle = N^{-1} \langle \psi_{k=0} \rangle. \quad (11)$$

In [18] equations (7) - (10) serve as the starting point for a diagrammatic expansion of $\rho(t)$ in powers of time. We now show how these relations may instead be used as the basis for an expansion of the stationary activity density $\rho_\infty \equiv \lim_{t \rightarrow \infty} \rho(t)$.

In writing equations (8) and (9) we have assumed a Poisson-product distribution, with expectation p , for the initial occupation numbers n_i . Thus $\langle \psi_{k=0} \rangle = Np$, a constant of the motion, since the number of particles is conserved. In the infinite-size limit, the law of large numbers implies that $N^{-1} \psi_{k=0} = p$, and is no longer a random variable. We may therefore isolate all terms with $k = 0$ in equation (9) setting each factor $N^{-1} \psi_{k=0}$ equal to p . (Observe as well that $\tilde{\psi}_{k=0}$, the variable conjugate to $\psi_{k=0}$, is no longer needed.) As a result of this procedure $\mathcal{G}[\psi, \tilde{\psi}]$ assumes the form

$$\mathcal{G}[\psi, \tilde{\psi}] \equiv \exp \left[-N^{-1} \int_0^t dt' \sum_{k \neq 0} (\tilde{\psi}_k \dot{\psi}_{-k} + \gamma_k \tilde{\psi}_{-k} \psi_k) + \int_0^t dt' \mathcal{L}'_I \right], \quad (12)$$

with

$$\gamma_k = 4p \omega_{-k,0} = 4p(1 - \cos k) \quad (13)$$

and the modified interaction

$$\begin{aligned} \mathcal{L}'_I = & -N^{-3} \sum_{k_1, k_2, k_3 \neq 0} \omega_{k_3, -k_1 - k_2 - k_3} \psi_{k_1} \psi_{k_2} \tilde{\psi}_{k_3} \tilde{\psi}_{-k_1 - k_2 - k_3} \\ & - 2pN^{-2} \sum_{k_1, k_3 \neq 0} \omega_{k_3, -k_1 - k_3} \psi_{k_1} \tilde{\psi}_{k_3} \tilde{\psi}_{-k_1 - k_3} - 2N^{-2} \sum_{k_1, k_2 \neq 0} \omega_{-k_1 - k_2, 0} \psi_{k_1} \psi_{k_2} \tilde{\psi}_{-k_1 - k_2} \\ & - p^2 N^{-1} \sum_{k_3 \neq 0} \omega_{k_3, -k_3} \tilde{\psi}_{k_3} \tilde{\psi}_{-k_3} \end{aligned} \quad (14)$$

(15)

Here it is understood that none of the wavevectors associated with the fields ψ and $\tilde{\psi}$ may be zero. The bilinear part of the action in equation (12) represents independent diffusion of particles at rate $4p$ [27]. The appearance of diffusion at rate $4p$ in \mathcal{L}_0 may be understood intuitively as follows. The rate of diffusion events at a given site is $n(n-1)$, i.e., twice the number of distinct pairs, so that the diffusion rate *per pair* is 2. The diffusion rate per particle is the twice the diffusion rate per pair times the number of pairs per particle, or $4(n-1) \simeq 4n \simeq 4p$ if $p \gg 1$. Unlike the original representation of equation (8), the important control parameter p now appears explicitly in the action, rather than being “hidden” in the initial probability distribution. It is worth noting that this reorganization of the action is not readily implemented in the operator representation, equation (3), because in this case it is the *operator* $N^{-1} \sum_i \pi_i a_i$ that assumes a fixed value p .

III. PERTURBATION EXPANSION

Let equation (12) with $\mathcal{L}'_I \equiv 0$ define \mathcal{G}_0 ; equation (7) with \mathcal{G}_0 in place of \mathcal{G} defines the free expectation $\langle \mathcal{A} \rangle_0$. Then for $k \neq 0$ we have [18]

$$\begin{aligned} \langle \psi_k(s) \rangle_0 &= 0 \\ \langle \tilde{\psi}_k(s) \rangle_0 &= 0 \end{aligned} \quad (16)$$

and the basic contraction or propagator is

$$\langle \psi_{k'}(u) \tilde{\psi}_k(s) \rangle_0 = N \delta_{k', -k} \Theta(u-s) e^{-\gamma_k(u-s)}, \quad (17)$$

where Θ represents the step function. As usual in this formalism, $\Theta(0) = 0$ [27]. The free expectation of n fields $\tilde{\psi}$ and n fields ψ is given by the sum of all possible products of n contractions.

The expectation of an observable can be written in the form

$$\langle \mathcal{A} \rangle = \left\langle \mathcal{A} e^{\int_0^t \mathcal{L}' dt'} \right\rangle_0 \quad (18)$$

which can be expressed in terms of free expectations if we expand the exponential. In this expansion, each field $\tilde{\psi}_k(\tau)$ must be contracted with a field $\psi_{-k}(\tau')$, with $\tau' > \tau$. At n -th order there is a factor of $1/n!$ and integrations $\int dt_1 \cdots dt_n$ over the interval $[0, t]$. We impose the time ordering $t \geq t_1 \geq t_2 \geq \dots \geq t_n \geq 0$, thereby cancelling the factor $1/n!$. We adopt a diagrammatic notation [18] in which fields $\psi(\tilde{\psi})$ are represented by lines entering (leaving) a vertex. All lines are directed to the left, the direction of increasing time. The first term in \mathcal{L}'_I , equation (14), corresponds to a vertex with four lines (“4-vertex”), the second and third to vertices with three lines (“3-vertex”), while the fourth, with two lines exiting, will be referred to as a “source.” figure 1 shows the vertices associated with \mathcal{L}'_I , as well as the “sink” corresponding to the observable ρ . Vertex b will be called a “bifurcation” and c a “junction”. In this way, the activity density

$$\rho = N^{-2} \sum_k \langle \psi_k \psi_{-k} \rangle = N^{-2} \sum_k \langle \psi_k \psi_{-k} e^{\int_0^t dt' \mathcal{L}'_I} \rangle_0 \quad (19)$$

takes the form

$$\begin{aligned} \rho &= +N^{-2} \langle \psi_{k=0}^2 e^{\int_0^t dt' \mathcal{L}'_I} \rangle_0 + N^{-2} \sum_{k \neq 0} \langle \psi_k \psi_{-k} e^{\int_0^t dt' \mathcal{L}'_I} \rangle_0 \\ &= p^2 + N^{-2} \sum_{k \neq 0} \langle \psi_k \psi_{-k} e^{\int_0^t dt' \mathcal{L}'_I} \rangle_0. \end{aligned} \quad (20)$$

Consider the first order term. From figure 1 it is evident that the only vertex that can be contracted with the sink (without leaving dangling lines) is the source. This *simple loop*, shown as the first diagram on the right hand side of figure 2, makes the contribution

$$\begin{aligned} &- 2p^2 N^{-1} \sum_k \omega_{k,-k} \int_0^t e^{-2\gamma_k(t-t_1)} \\ &= \frac{p}{4} \int_{-\pi}^{\pi} \frac{dk}{2\pi} (1 + \cos k) [e^{8p(1-\cos k)t} - 1] \\ &= \frac{p}{4} \left\{ e^{-8pt} [I_0(8pt) + I_1(8pt)] - 1 \right\}. \end{aligned} \quad (21)$$

where the prefactor 2 is a combinatorial factor and I_ν denotes the modified Bessel function. Here we used

$$N^{-1} \sum_k \xrightarrow{N \rightarrow \infty} \int_{-\pi}^{\pi} \frac{dk}{2\pi}. \quad (22)$$

Thus this diagram yields the contribution identified in Ref. [18] as $\rho_{max}(t)$, the sum of all contributions at order $n = 1, 2, 3, \dots$ proportional to p^{n+1} , the highest power of p allowed at a given order. In the limit $t \rightarrow \infty$ the contribution to the activity from this term is $-p/4$.

To study the stationary regime it is convenient to use the Laplace transform. For example, the Laplace transform of the contribution due to the simple loop, equation (21), is

$$-\frac{2p^2}{s} \int_{-\pi}^{\pi} \frac{dk}{2\pi} \frac{1 - \cos^2 k}{s + 8p(1 - \cos k)} \quad (23)$$

where s denotes the transform variable. Using the property $\lim_{t \rightarrow \infty} f(t) = \lim_{s \rightarrow 0} s\tilde{f}(s)$, we obtain the limiting contribution $-p/4$ directly.

Consider an arbitrary diagram D of n vertices, and denote the time-dependent factors in its contribution to $\rho(t)$ by $f_D(t)$. The Laplace transform of this contribution has the form

$$\begin{aligned} \tilde{f}_D(s) &= \int_0^\infty dt e^{-st} \int_0^t dt_1 \int_0^{t_1} dt_2 \dots \int_0^{t_{n-1}} dt_n e^{-\alpha_1(t-t_1) - \alpha_2(t_1-t_2) \dots - \alpha_n(t_{n-1}-t_n)} \\ &= \int_{t_1}^\infty dt \int_{t_2}^\infty dt_1 \dots \int_0^\infty dt_n e^{-(\alpha_1+s)(t-t_1) - (\alpha_2+s)(t_1-t_2) \dots - (\alpha_n+s)(t_{n-1}-t_n) - st_n} \\ &= [s(\alpha_1 + s)(\alpha_2 + s) \dots (\alpha_n + s)]^{-1}, \end{aligned} \quad (24)$$

where the α_i are functions of the wavevectors. Then we have

$$\bar{f}_D \equiv \lim_{t \rightarrow \infty} f_D(t) = \prod_{i=1}^n \frac{1}{\alpha_i}. \quad (25)$$

The factors α_i may be determined via the following procedure. Draw the diagram with all vertices in order, and draw vertical lines through each vertex. Then α_i is the sum of the factors γ_q for all propagators between the vertical lines associated with vertices i and $i-1$ (here $t = 0 \equiv t_0$), *regardless of whether or not these propagators link vertices i and $i-1$.*

For example, a diagram composed of n simple loops (see figure 2) makes a contribution of

$$\frac{(-1)^n 2^n p^2}{s} \left[\int_{-\pi}^{\pi} \frac{dk}{2\pi} \frac{1 - \cos^2 k}{s + 8p(1 - \cos k)} \right]^n, \quad (26)$$

to $\tilde{\rho}(s)$, and so its contribution to ρ_∞ is

$$\frac{(-1)^n 2^n p^2}{(8p)^n} = (-1)^n p^2 \frac{1}{(4p)^n}. \quad (27)$$

Summing on n , we find the contribution due to this sequence of diagrams to the reduced activity $\bar{\rho} \equiv \lim_{t \rightarrow \infty} (\rho/p^2)$:

$$\sum_{n=1}^{\infty} \left(\frac{-1}{4p} \right)^n = -\frac{1}{1+4p} \equiv -\kappa. \quad (28)$$

In certain cases it is straightforward to replace a simple loop with the infinite sum of 1, 2, 3, ... loops. This procedure, illustrated graphically in figure 2, will be called *dressing* a loop.

Figure 3 shows a three-vertex diagram not included in the sequence equation (28). It makes the following contribution to $\bar{\rho}$:

$$\frac{-32p}{4p(8p)^2} \int_{-\pi}^{\pi} \frac{dk}{2\pi} (1 + \cos k) \int_{-\pi}^{\pi} \frac{dq}{2\pi} \frac{1 - \cos q \cos(k - q)}{3 - \cos q - \cos k - \cos(k - q)}. \quad (29)$$

The integral over wavevector q arises frequently in the diagrammatic series and can be evaluated in closed form:

$$\begin{aligned} I(k) &= \int_{-\pi}^{\pi} \frac{dq}{2\pi} \frac{1 - \cos q \cos(k - q)}{3 - \cos q - \cos k - \cos(k - q)}. \\ &= \frac{1}{2} \left[\frac{3 - c - \sqrt{(1-c)(7-c)}}{1+c} + \sqrt{\frac{1-c}{7-c}} \right] \end{aligned} \quad (30)$$

where c denotes $\cos k$.

In any diagram (beyond the set included in figure 2), we may insert any number of loops immediately to the right of the sink. That is, the sink may be replaced by a dressed loop. The same applies to the rightmost source, vertex n . The result is that the contribution of the original diagram is multiplied by $[4p/(1+4p)]^2$. Once this factor is included, no diagram with a 4-vertex immediately to the left of the rightmost source (i.e., in position $n-1$) or immediately to the right of the sink (position 1) need be included in the series.

IV. DIAGRAMMATIC ANALYSIS

To begin we define the rules for constructing diagrams in the series for $\bar{\rho}$ [18]. [Since there is exactly one factor of N^{-1} associated with each wavevector sum, all of the latter may be changed to integrals, using equation (22).]

1. Draw all connected diagrams of n vertices and a sink to the left of all vertices; the rightmost vertex must be a source. Each line exiting vertex j must be contracted with a line entering some vertex $i < j$. There is a factor $\delta_{k',-k}$ associated with each such internal line, where k is the wavevector exiting vertex j and k' the wavevector entering vertex i . The requirement that all lines be contracted leads to the condition $2(n_s - 1) + n_b - n_c = 0$, where n_s is the number of sources, n_b the number of bifurcations, and n_c the number of junctions.

2. Each diagram possesses a factor of $(-1)^n$ and a combinatorial factor reflecting the number of ways of realizing the contractions. In the series for $\bar{\rho}$, this factor is given by 2^C , with $C = 1 + n_3 + 2n_4 + n_s - \ell$, where n_3 is the number of 3-vertices (of either kind), n_4 the number of 4-vertices, and ℓ the number of simple loops.

3. Associated with each bifurcation is a factor $2p\omega_{k_1,k_2} = 2p[1 - \cos k_1 \cos k_2]$. Each junction carries a factor $2\omega_{k,0}$ and each 4-vertex a factor ω_{k_1,k_2} . Each source carries a factor of $p^2\omega_{k,-k}$. (The k_i denote the wavevectors exiting the vertex.)

4. There is a factor \bar{f}_D resulting from the time integrations, as discussed above.

5. Replace the sink and rightmost source with dressed loops, leading to the factor $[4p/(1+4p)]^2$ mentioned above, and exclude all diagrams with a 4-vertex in position 1 or $n-1$.

6. Integrate over all wavevectors.

Collecting the factors of p and $1/p$ associated with the various vertices, \bar{f}_D , and the factor of p^{-2} in the definition of $\bar{\rho}$, we find that each diagram in the series for $\bar{\rho}$ contains an overall factor p^{-r} where $r = n - n_b - 2(n_s - 1)$. Using the relation $2(n_s - 1) + n_b - n_c = 0$, we have $r = n - n_c$.

In order to take advantage of our simple results for the sum of an infinite set of diagrams represented by the dressed loops, we adopt $\kappa \equiv (1+4p)^{-1}$ as the expansion parameter rather than p . Noting that $4p/(1+4p) = 1 - \kappa$, and that $1/p = 4\kappa/(1 - \kappa)$, we see that the first order diagram (i.e., the single dressed loop of figure 2) carries a factor of $4/(1+4p) = 4\kappa$, while diagrams at higher order carry a factor $[4p/(1+4p)]^2$, so that at order $1/p^r$ there is an overall factor of $(4\kappa)^r/(1 - \kappa)^{r-2}$. Thus diagrams $\propto \kappa^r$ contribute at order r and all higher orders. Diagrams in this class must have at least $r + 1$ vertices and no more than $3r - 2$ vertices.

Enumeration of diagrams at a given order involves (1) identifying all allowable sequences of n vertices, and (2) identifying all possible sets of connections between vertices, for each sequence. For diagrams with $n \geq 3$ (i.e., those not included in the simple dressed loop of figure 2), vertex 1 (nearest the sink) must be a junction. (As explained above it cannot be a 4-vertex. If it were a bifurcation, the wavevector of the single line entering this vertex would of necessity be zero, but such terms have been excluded from the action.) For similar reasons, vertex $n - 1$ must be either a source or a bifurcation. Once the vertex sequence has been fixed, all possible sets

of contractions of outgoing and incoming lines must be enumerated. The single line exiting vertex 1 must, naturally, always terminate at the sink.

The enumeration of sequences and connections is readily codified in an algorithm that may be implemented via computer. In our routine, for each n and r , all sequences (subject to the above limitations) are constructed. Then all possible connections are generated, by simply running through all termination points for each line independently, and rejecting those sets that result in uncontracted lines. In this way we are able to enumerate all the diagrams at a given order.

A diagram is specified in terms of its *bond set* $\{(v_1, v'_1), \dots, (v_m, v'_m)\}$, where v_j and $v'_j > v_j$ are the terminal vertices of line j , with $j = 0$ for the sink. Thus the diagram of figure 3 can be written: (01) (12) (12) (23) (03). (The computer algorithm was verified against hand enumeration up to third order.) Since the number of diagrams grows very rapidly, we extended the routine to perform the wavevector integrations for each diagram generated. This entails construction of the numerator and denominator of the integrand, which are products of factors involving the cosines of various linear combinations of wavevectors. The numerator is a product of factors associated with each vertex, as noted in item 3 above. The denominator is a product of factors associated with each interval between vertices. These factors are readily determined, given the vertex sequence and set of connections. Note that there is one free wavevector k_i associated with each vertex, except for junctions, so that the number of wavevector sums is r . In the latter case the wavevector exiting is equal to the sum K of those entering. The lines exiting a source carry wavevectors k' and $-k'$, where k' denotes the new associated wavevector. In the case of a bifurcation or a 4-vertex we may take the wavevectors of the lines exiting as k' and $K - k'$ where K denotes the wavevector entering (or the sum of the wavevectors entering, in the case of a 4-vertex). Thus we see that the construction of the integrand (including associated numerical factors) is a straightforward task that can also be codified in a computational algorithm. The integrals over the k_i are evaluated numerically using a midpoint method [31]. Based on results for varying number of intervals in the numerical integration, we are able to determine the resulting coefficients with a relative uncertainty of about 10^{-4} or less.

V. RESULTS

We have carried out the expansion for $\bar{\rho}$ to order κ^4 . Call the number of n -vertex diagrams at order κ^r $N_{n,r}$ and the contribution of this set of diagrams to the coefficient of $\kappa^r/(1 - \kappa)^{r-2}$ in this series $b_{n,r}$; these values are reported in Table I.

The diagrammatic expansion yields the following expression for the stationary activity density

$$\bar{\rho}_\infty = 1 - \kappa - 1.788\,040\kappa^2 - 4.414\,481\kappa^3 - 14.632(2)\kappa^4 + \mathcal{O}(\kappa^5) \quad (31)$$

In figure 4 we compare equation (31) and the results of Monte Carlo [19] simulations using systems of up to 800 sites. (For each p value, simulations are performed for various system sizes and the results extrapolated to the infinite-size limit.) For $p \geq 3$ the difference between the series expression and simulation is less than 0.1%. In Ref. [19], a similar degree of precision is obtained by extrapolating (using Padé approximants) a 16-term series (in powers of t) to the infinite-time limit. The present series of four terms appears to furnish (without transformation or extrapolation), information equivalent to that obtained from a much longer series in powers of t . It is worth noting that while the time series is divergent, the present series appears to be convergent for small values of κ , and it is natural to interpret the first singularity on the positive- κ axis as marking the phase transition.

With a series of only four terms it is of course difficult to draw firm conclusions regarding the location of the critical point. We nevertheless analyze the series via Padé approximants [32]. The [2,2] approximant is the best behaved and is in excellent accord with simulation for $p \geq 1.5$. It yields a critical value of $p_c = 0.8677(3)$. (The [1,3] and [3,1] approximants give $p_c = 0.668$ and 0.702 , respectively.) It is usual to analyse the Padé approximant to the series for the derivative of the logarithm of the order parameter ($d \ln \bar{\rho} / d\kappa$ in the present instance), as this function should exhibit a simple pole at the critical point. The [2,1] approximant does in fact give an improved estimate of $p_c = 0.9069$ (about 5% below the value found in simulations), while the [1,2] approximant yields $p_c = 0.860$. (The residue at the pole of the [2,1] approximant is 0.198, well below any of the numerical estimates for the critical exponent β that have been reported, which suggest $\beta \simeq 0.4$ [12–14].) The series prediction is compared against simulation in figure 4. For $p \geq 3$, series and simulation agree to within uncertainty, i.e., with a relative error of 10^{-4} . We note that the four-term series for the stationary activity yields results of accuracy comparable to that obtained from the 16-term series in powers of time. The latter, when extrapolated to $t = \infty$, gives $p_c = 0.906$ [19].

The chief barrier to extending the series is the rapid growth in the cpu time required in evaluating the multiple integrals over wavevectors, combined with the explosive growth in the number of diagrams. (Enumeration of the diagrams represents a small fraction of the computing time.) Thus the present approach does not appear viable for r greater than four.

For similar reasons the analysis of the two-dimensional case is restricted to $r \leq 3$. As explained in Ref. [18], the formalism remains valid in d dimensions if we replace all factors $\omega_{k,k'}$ with

$$\omega_{\mathbf{k}_1, \mathbf{k}_2} = 1 - \lambda_d(\mathbf{k}_1)\lambda_d(\mathbf{k}_2), \quad (32)$$

where

$$\lambda_d(\mathbf{k}) \equiv \frac{1}{d} \sum_{\alpha=1}^d \cos k_\alpha. \quad (33)$$

Thus $\gamma_{\mathbf{k}}$ in equation (13) becomes

$$\gamma_{\mathbf{k}} = 4 p [1 - \lambda_d(\mathbf{k})] . \quad (34)$$

The expansion involves the same set of diagrams in any dimension; only the integrals change, with the wave vectors now ranging over the first Brillouin zone in d dimensions.

In two dimensions our result for the stationary activity density is:

$$\bar{\rho}_{\infty} = 1 - \kappa - 1.704155\kappa^2 - 3.7292\kappa^3 + \mathcal{O}(\kappa^4) \quad (35)$$

The series prediction is compared against Monte Carlo simulation in figure 5; good agreement is observed for $p \geq 1.5$. The [2,1] and [1,2] Padé approximants to the three-term series for $\bar{\rho}$ yield critical values of $p_c = 0.507$ and 0.502 respectively, whereas the estimate from simulation is 0.715 .

VI. CORRELATION FUNCTIONS AND PROBABILITY DISTRIBUTION

Consider the stationary expectation $\langle n_j n_{j+\ell} \rangle$ of the product of occupations at sites j and $j + \ell$. For $\ell \neq 0$ this may be written as [18]:

$$C(\ell) \equiv N^{-1} \sum_j \langle n_j n_{j+\ell} \rangle = N^{-2} \sum_k e^{ik\ell} \langle \psi_k \psi_{-k} \rangle \quad (36)$$

and separating the $k = 0$ term as in equation (20) we find

$$C(\ell) = p^2 + N^{-2} \sum_{k \neq 0} \cos k\ell \langle \psi_k \psi_{-k} e^{\int_0^t dt' \mathcal{L}'_t} \rangle_0 \quad (37)$$

The second term, an infinite sum of diagrams, defines the connected two-point correlation function $G(|\ell|)$. The lowest order contribution comes from the one-vertex diagram (simple loop) giving

$$G^{(1)}(|\ell|) = -\frac{p}{4} \int_{-\pi}^{\pi} \frac{dk}{2\pi} \cos k\ell (1 + \cos k), \quad (38)$$

or $G^{(1)}(1) = -p/8$ and $G^{(1)}(|\ell|) = 0$ for $|\ell| > 1$. When the dressed loop is evaluated this becomes $G^{(1)}(1) = -\kappa p^2/8$. The correlation for sites separated by greater than unit distance is $\mathcal{O}(\kappa^2)$ or higher. From this result we can draw the following conclusions: (1) The nearest-neighbor correlation is negative for large p ; (2) For large p correlations decay rapidly in space; (3) As $p \rightarrow \infty$, the reduced correlation

$\overline{G}(\ell) = G(\ell)/p^2$ decays to zero (as $1/p$ or faster) so that in this limit the site occupancies are independent random variables.

The stationary expectation of $(\psi_j)^m$ (product of m fields at the same site) is related to the m -th factorial moment of the one-site occupation distribution. [For $m = 2$ this is seen explicitly in equation (10).] For $m = 3$ for example, we have

$$\langle n^3 \rangle_F \equiv N^{-1} \sum_j \langle n_j(n_j - 1)(n_j - 2) \rangle = N^{-3} \sum_{k,k'} \langle \psi_k \psi_{k'} \psi_{-k-k'} \rangle \quad (39)$$

which can be written

$$\langle n^3 \rangle_F = p^3 + 3pN^{-2} \sum_{k \neq 0} \langle \psi_k \psi_{-k} \rangle + N^{-3} \sum_{k,k' \neq 0} \langle \psi_k \psi_{k'} \psi_{-k-k'} \rangle \quad (40)$$

The second term equals $3p(\rho - p^2)$ and so is $\mathcal{O}(p^2)$ for large p . The third term must be expanded in diagrams in which the sink has *three* lines entering. The lowest order diagram thus involves two vertices, a source and a bifurcation, and is $\mathcal{O}(p)$ for large p . We see then that $\langle n^3 \rangle_F = p^3[1 + \mathcal{O}(1/p)]$ for large p . The same line of reasoning shows that the m -th factorial moment approaches p^m as $p \rightarrow \infty$. In this limit the one-site marginal distribution is therefore Poisson with parameter p , and by our previous result on independence, the joint probability distribution is a product of such distributions.

We defer a detailed analysis of correlation functions to future work, and stress that the main result of the present section is that in the large- p limit, the probability distribution is a product of identical Poisson distributions at each site, as was conjectured in [19]. It is readily seen that this remains valid in $d \geq 2$ dimensions.

VII. DISCUSSION

We derive a path-integral representation and diagrammatic expansion for the stationary activity density in a stochastic sandpile with a conserved particle density. Because of conservation, the $k = 0$ Fourier mode of the particle density (and associated field ψ_k) has a fixed value, rather than being a random variable. This observation permits us to reorganize the effective action so that the control parameter p appears explicitly, rather than being defined implicitly in the initial condition. The bilinear part of the action now describes diffusion at a rate $4p$. Because of this, the propagator carries an exponential factor, and all time integrations can be realized to obtain the limiting ($t \rightarrow \infty$) activity directly. The ensuing expansion for $\overline{\rho}_\infty$ involves the parameter $\kappa = (1 + 4p)^{-1}$, i.e., this is a large- p expansion. (As noted in Ref. [19], the time series is also most useful for large p values.) We are able to sum certain infinite classes of diagrams through the device of “dressed loops.” Despite this, the number of diagrams to be evaluated at each order grows explosively, so that our final

calculational result (the activity series to $\mathcal{O}(\kappa^4)$) is quite modest. The fourth-order series agrees very well with simulation in the supercritical regime, and yields (via Padé approximation) the critical value p_c to within about 10%. A similar favorable comparison is seen in the two-dimensional case, although the three-term series furnishes a poorer estimate for p_c . Given these encouraging results, it is reasonable to hope that extended series will yield quantitative predictions for critical properties. We have also used the reorganized expansion to show that in the large- p limit, the sandpile is governed by Poisson-product distribution. Our results strengthen the conclusion, until now based on simulation and mean-field-like analyses, that fixed-energy sandpiles exhibit a phase transition as the particle density is varied. It is of great interest to know if the details of this transition can be analysed using the operator and path-integral formalisms.

ACKNOWLEDGMENTS

We are grateful to Miguel A. Muñoz for valuable comments on the manuscript. This work was supported by CNPq and CAPES, Brazil.

REFERENCES

- [1] P. Bak, C. Tang and K. Wiesenfeld, Phys. Rev. Lett. **59**, 381 (1987); Phys. Rev. A **38**, 364 (1988).
- [2] D. Dhar, Physica A **263**, 4 (1999) and references therein.
- [3] G. Grinstein, *Scale Invariance, Interfaces and Nonequilibrium Dynamics (NATO Advanced Study Institute, Series B: Physics vol 344)* ed. A McKane et al. (Plenum Press, New York, 1995).
- [4] D. Sornette, A. Johansen and I. Dornic, J. Physique I **5**, 325 (1995).
- [5] A. Vespignani and S. Zapperi, Phys. Rev. Lett. **78**, 4793 (1997). A. Vespignani and S. Zapperi, Phys. Rev. E **57**, 6345 (1998).
- [6] R. Dickman, A. Vespignani and S. Zapperi, Phys. Rev. E **57**, 5095 (1998).
- [7] J. Marro and R. Dickman, *Nonequilibrium Phase Transitions in Lattice Models* (Cambridge University Press, Cambridge, 1999).
- [8] H. Hinrichsen, Adv. Phys. **49**, 815 (2000).
- [9] Braz. J. Phys. **30**, no. 1, (2000).
- [10] A. Vespignani, R. Dickman, M. A. Muñoz and S. Zapperi, Phys. Rev. E **62**, 4564 (2000).
- [11] M. Rossi, R. Pastor-Satorras and A. Vespignani, Phys. Rev. Lett. **85**, 1803 (2000).
- [12] R. Dickman, M. Alava, M. A. Muñoz, J. Peltola, A. Vespignani and S. Zapperi, Phys. Rev. E **64**, 56104 (2001).
- [13] R. Dickman, T. Tomé and M. J. de Oliveira, Phys. Rev. E **66**, 16111 (2002).
- [14] S. Lübeck, Phys. Rev. E **65**, 046150 (2002); *ibid* **66**, 046114 (2002).
- [15] S. Lübeck and P. C. Heger, Phys. Rev. Lett. **90**, 230601 (2003); Phys. Rev. E **68**, 056102 (2003).
- [16] V. B. Priezhev, E. V. Ivashkevich, A. M. Povolotsky and C.-K. Hu, Phys. Rev. Lett **87**, 84301 (2001).
- [17] S. Maslov and Y. C. Zhang, Phys. Rev. Lett **75**, 1550 (1995).
- [18] R. Dickman and R. Vidigal, J. Phys. A **35**, 7269 (2002).
- [19] J. Stillek, R. Dickman and R. Vidigal, J. Phys. A **37**, 1145 (2004).
- [20] M. Doi, J. Phys. A **9**,1465,1479 (1976).
- [21] R. Dickman, J. Stat. Phys. **55**, 997 (1989).
- [22] R. Dickman and I. Jensen, Phys. Rev. Lett. **67**, 2391 (1991).
- [23] I. Jensen and R. Dickman, J. Stat. Phys. **71**, 89 (1993).
- [24] R. Dickman, J-S Wang and I. Jensen, J. Chem. Phys. **94**, 8252 (1991). M. J. De Oliveira, T. Tomé and R. Dickman, Phys. Rev. A **46**, 6294 (1992).
- [25] J. Zhuo, S. Redner and H. Park, J. Phys. A **26**, 4197 (1993).
- [26] L. Peliti, J. Physique **46**,1469 (1985).
- [27] R. Dickman and R. Vidigal, Braz. J. Phys. **33**, 73 (2003).
- [28] S. S. Manna, J. Phys. A:Math. Gen. **24**, L363 (1991).
- [29] S. S. Manna, J. Stat. Phys. **59**, 509 (1990).
- [30] R. Dickman, unpublished.
- [31] The enumeration/integration code is available on request to the authors.

- [32] G. A. Baker, *Quantitative Theory of Critical Phenomena* (Academic Press, New York, 1990).

TABLES

n	r	$N_{n,r}$	$b_{n,r}$
3	2	2	-2.384 052
4	2	3	0.596 013
4	3	4	5.625 989
5	3	49	-19.520 916
6	3	180	11.376 647
7	3	306	-1.896 110
5	4	8	-13.225 188
6	4	311	135.895 511
7	4	3 471	-311.353
8	4	21 961	256.075
9	4	76 261	-88.685
10	4	136 404	11.092

Table I. Number of diagrams $N_{n,r}$ and coefficient $b_{n,r}$ in the expansion of the activity.

FIGURE CAPTIONS

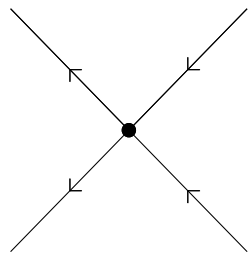
Figure 1. Vertices (a - d) in the interaction \mathcal{L}' and the sink (e) representing the activity density.

Figure 2. Definition of a “dressed loop” as the sum of one, two, three,... simple loops joined at 4-vertices.

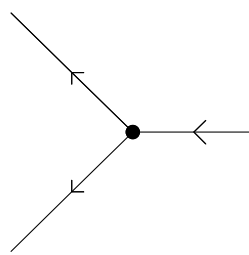
Figure 3. A three-vertex diagram.

Figure 4. Scaled stationary activity density $\bar{\rho}$ versus particle density p in one dimension. Upper curve: series prediction, equation (31); the curve labeled [2,1] is obtained by integrating the Padé approximant to the series for $d \ln \bar{\rho} d\kappa$; points: Monte Carlo simulation. Error bars are smaller than the symbols.

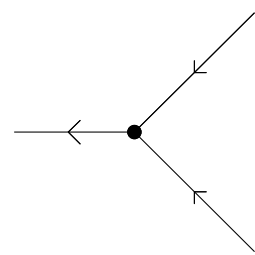
Figure 5. Scaled stationary activity density $\bar{\rho}$ versus particle density p in two dimensions. Upper curve: series prediction, equation (35); lower curve: [2,1] Padé approximant to the series; points: Monte Carlo simulation.



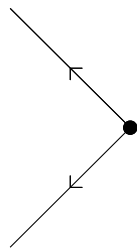
a



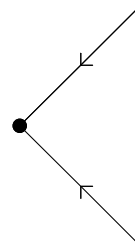
b



c



d



e

